JELECHEM-D-16-00221 R1

Regular paper manuscript for publication consideration in
Journal of Electroanalytical Chemistry

SI: Prof. Koichi Aoki

Potential-dependent morphological change of *n*-hexadecane small droplets on a Au(1 1 1) electrode in aqueous solution: a voltammetric and electrochemical fluorescence microscopic study

Tetsuro Morooka[a], Shoma Murakawa[b], Azusa Konomi[b], Daisaku Goto[b], Takamasa Sagara[c,*]

[a] *Department of Advanced Technology and Science for Sustainable Development, Graduate School of Engineering, Nagasaki University, Bunkyo 1-14, Nagasaki 852-8521, Japan.*
[b] *Department of Materials Engineering and Molecular Science, Graduate School of Engineering, Nagasaki University, Bunkyo 1-14, Nagasaki 852-8521, Japan.*
[c] *Division of Chemistry and Materials Science, Graduate School of Engineering, Nagasaki University, Bunkyo 1-14, Nagasaki 852-8521, Japan.*

Keywords: *Alkane droplet, Au(1 1 1) electrode, Electrochemical fluorescence microscopy Potential-driven dynamics, Surface tension, Spreading*

♦dedicated to Prof. Koichi Aoki in honor of his profound contributions to analytical electrochemistry.

* Corresponding author.
E-mail address: sagara@nagasaki-u.ac.jp (T. Sagara)
URL: http://www.cms.nagasaki-u.ac.jp/lab/douteki/en/index.html

Abstract

A mesoscopic view of active droplets of an alkane on a Au(1 1 1) electrode was described using the results of voltammetric and *in situ* electrochemical fluorescence imaging measurements. *In situ* fluorescence imaging studies revealed that the morphology of an adlayer of liquid *n*-hexadecane (HD) on a Au(1 1 1) electrode surface is reversibly driven by potential, forming micro-droplets with greater height of the droplet's top at more negative potentials. Spreading of HD to be a continuous liquid film never took place even around pzc and even with the amounts of HD ranging from 10 to 10000 monolayer equivalent. The droplets at negative potentials were smaller than 50 μm in diameter. The total Au electrode area occupied by HD was small even at positive potentials so that quasi-reversible redox reaction of ferri/ferro-cyanide in the solution phase was still observed. The change of the droplet height by the reshaping with the electrode potential was repeatable, and the change took place beyond the double layer thickness region.

Highlights

- *n*-Hexadecane (HD) on the Au(1 1 1) electrode surface exists as small droplets but never covers the surface as a continuous liquid film.
- The size of HD droplet deposited on a Au(1 1 1) surface by a touching method was smaller than 50 μm in diameter.
- The height of the HD droplet top rises beyond the double layer thickness on the electrode surface around –0.55 V.
- The HD droplets on the electrode surface are not the obstacle to the quasi-reversible redox reaction of solution-phase ferri/ferro-cyanide.

1. Introduction

Potential driven dynamics of organic molecules, not only those forming ordered adlayers on an electrode surface but also those covering it as liquids, provide us with rich perspectives of electrochemistry and molecular organization chemistry in aqueous media. Amphiphiles such as surfactants bearing a long alkyl chain often form adlayers that exhibit potential dependent reversible phase changes on an electrode surface [1-5]. The phase changes include adsorption-desorption and orientation change of molecules, two-dimensional (2D) phase transition to form a condensed monolayer, and ingress/egress of water molecules into/from the adlayer. The organic liquid, the droplet of which exhibits potential dependent morphological change and reshaping, is represented by alkanes. A liquid droplet on a substrate has been subject to voltage control after the pioneering work of Gabrial Lippmann on the electrowetting [6]. In addition to the conductive droplets placed on a thin insulator film-covered electrode in a gas phase under voltage control, the non-conductive droplets directly placed on an electrode surface in an electrolyte solution have been also subject to active electrochemical control, as exemplified by non-faradaic control [7] and faradaic control [8]. The understanding of the behavior of liquid alkanes is inevitable to describe the dynamics of adlayers of alkyl substances, because it is a key element to understand the movements of the alkyl chains, each molecule, and an assembly of the molecules [1]. Note that, in contrast to a liquid lens on a thin insulator needed application over 30 V for the active control, direct potential control of the adlayers and droplets can be made much less than a voltage amplitude of 3 V in an electrolyte solution.

We herein focus on the dynamics of alkanes as insulating oils on a Au(1 1 1) electrode surface in aqueous solutions. Because a Au(1 1 1) surface has rather low surface energy and high stability in a wide electrochemical window, it appears the substrate of choice in many studies to place an oil droplet or to adsorb alkane molecules on it. We may have two different ways to view the alkanes on the electrode surface; one is a molecular view and the other is a continuum liquid phase view.

In the molecular view, alkane molecules are regarded as adsorbates at an electrode/aqueous solution or electrode/liquid alkane interface. They have been the targets of *in situ* electrochemical scanning tunneling microscopy (EC-STM). Uosaki and Yamada showed the formation of the 2D crystal of normal alkanes (C16, 17) on Au(1 1 1) surface/neat alkane liquid

interfaces as STM images [9]. They observed a herringbone structure and a row structure (lamella) crossing the herringbone. Several systematic studies of Au(1 1 1) surfaces in contact with neat liquids or solutions of normal alkanes (C14-38) using (EC-)STM revealed the structures of flat-lying ordered adlayers of the alkanes [10-15]. The ordered structure originates in the interaction between the hydrocarbon chain and the Au(1 1 1) surface lattice. An alkanol monolayer (C10-30) also takes the titled lamellar structure and the herringbone-like structure [16]. He and colleagues showed that an order-disorder transition of *n*-hexadecane molecules in a monolayer at a Au(1 1 1) electrode surface is induced by the electrode potential [17]. Around the potential of zero charge (pzc), observed was a highly ordered flat-lying hexadecane monolayer, which disappeared at the negatively and positively charged electrode surfaces. Such a potential dependent change of the state of the adlayer results from competitive adsorption of alkane molecules to water molecules and electrolyte ions.

In the view of a continuum liquid phase, Inošević and Žutić photographically sketched out the typical electrochemical behavior of a macroscopic liquid (75 μL) droplet of *n*-hexadecane at a Hg pool electrode in aqueous phase [7,18]. Hexadecane and other organic liquids immiscible with water tended to spread on the Hg surface around pzc but to bear off from the surface at negative potentials. They demonstrate spectacular amplitude of reversible morphological change as a function of the electrode potential. The potential dependent interfacial balance at three-phase contact line, water, oil, and electrode, represented by the Young's equation [19], is usually the model of the first choice to describe the oil droplet reshaping. Gorman and colleagues used a hexadecanethiol droplet (~1 μL) placed on a transparent poly-crystalline Au film electrode [20]. They demonstrated the control of the shape of the droplet using electrochemical reductive desorption and re-adsorption of the thiol molecules in the potential range width of 1.7 V in 0.1 M $NaClO_4$ solution. This potential-driven dynamics may find application to electrochemical switching of an optical lens. Nagai and coworkers changed a macroscopic contact angle of a *n*-hexane droplet (1 μL) at the atomically flat Au or Pt(1 1 1) electrode/H_2SO_4 aqueous solution interface by driving it through the potential dependent structure of adsorbed water molecules at the electrode surface [21]. This work demonstrates the importance of water molecular adsorption at the edge of the droplet in the potential driving.

Electrochemical control of movement of insulating droplets was studied on surface-modified electrode surfaces as exemplified by a 1,2-dichloroethane droplet (2 μL) on a polypyrrole

film-coated Au on a silicon wafer in an aqueous solution [22] and a nitrobenzene (NB) droplet (over 1 mm-diameter) at a SAM of a ferrocene compound having a wetting gradient produced by its redox reaction [23]. Ionic-conductive or redox-active oil droplets were also the target of electrochemical control as exemplified by a 0.1 μL NB droplet containing tetrabutylammonium tetraphenylborate on a Au electrode to achieve low-voltage electrowetting [24] and a 3 cm^3 NB droplet containing ferrocene on a glassy carbon electrode [25], both in aqueous electrolyte solution. On the other hand, the use of electrode surface coatings with insulator films was investigated in two-electrode electrowetting systems to control water or aqueous electrolyte solution droplets by voltage application [26-29], including the use of epoxy [27] and Teflon [28,29] at the outermost surfaces.

All the droplet studies fall in the volume range between 0.1 μL to 0.5 mL or 3 cm^3, whereas molecular views are on literally a nanometer scale. Mesoscopic level studies of the potential-driven dynamic are thus indispensable especially to bridge the two separate scales and to develop the method of dynamic control. In the mesoscopic domain, pico-liter (pL) size droplets are of particular importance in printing technology and cell biological medicine.

The aim of this work is to describe the dynamics of liquid *n*-hexadecane at a single crystal Au(1 1 1) electrode/aqueous electrolyte solution interface at a mesoscopic level in response to ca. 1 V change of the electrode potential. The dynamics of alkanes at a mesoscopic level should be described by both morphological change controlled by changing the interfacial tension balance at the macroscopic three-phase contact line and molecular-level direct interaction between alkane molecules and electrode surface atoms. Analysis of the dynamics of alkanes at a mesoscopic level is, therefore, expected to gain new perspectives, for example, the state of disordered *n*-alkane monolayers at negative potentials, characteristics of the liquid adlayer of a several monolayer level amount, and relevance to the redox processes. Experiments at a mesoscopic level are required for in-depth understanding of unclarified dynamic behavior and for elucidation of factors of the potential dependent behaviors.

The main approach in this work to track the potential-driven movements of the liquid is the use of *in situ* electrochemical fluorescence microscopy for real time imaging of the electrode/solution interface under potential control. It enables us not only to figure out 2D morphologies on the electrode surface in the optical microscopic scales but also to detect the movement of the probe dye molecules in the surface-normal direction. Effective applications of

in situ fluorescence microscopic video imaging to electrified interfaces have recently been demonstrated [30,31]. To mention just few examples, Musgrove and coworkers successfully used the fluorescence microscopic video imaging technique to investigate both reductive and oxidative desorption of a fluorophore-labeled alkyl thiol SAM at a Au electrode [32]. Shepherd and coworkers studied the potential-induced desorption and re-adsorption of the surfactant dye film [33,34]. Quenching of the fluorescence in close proximity to a metal electrode surface suppresses its intensity so greatly [30,35] that imaging at the monolayer thickness has been regarded as difficult. The fluorescence intensity depends on the distance between the fluorophore and a metal electrode surface in the range up to 50 nm and farther [30,35-38]. Turning this fact to an advantage, one can track the movement of probe dye molecules normal to the electrode surface while attaining 2D information. Based on these developments, the *in situ* electrochemical fluorescence studies have found a variety of measurement applications [39-42].

2. Experimental

2.1. Materials

n-Hexadecane (HD) was of reagent grade from Tokyo Kasei Kogyo Co. (Japan). The purity of HD was checked by UV-vis absorption and fluorescence spectra to affirm the absence of light absorbing or emitting impurity. Water was purified through a Milli-Q integral (Millipore) to a resistivity over 18 MΩ cm. Potassium perchlorate ($KClO_4$) of the highest reagent grade from Wako Pure Chemical Industries (Japan) was recrystallized three times from water and was dried in vacuo. Both potassium hexacyanoferrate(III) of reagent grade from Wako Pure Chemical Industries (Japan) and potassium bicarbonate of Cica-reagent grade from Kanto Chemical Co. (Japan) were used as received. Fluorescence probe dyes, 1,6-diphenyl-1,3,5-hexatriene (DPH) of a liquid scintillation grade from Nacalai Tesque Inc. (Japan) and perylene (Pr) of the highest reagent grade from Kanto Chemical Co. (Japan), were used as received. (The fluorescence and excitation spectra of these two dyes are found in Fig. S1 in Supplementary Data.) All other chemicals were of the highest reagent grade commercially available and were used as received.

A rod of cylindrical single crystal Au with a (1 1 1) base with a surface area of A = 0.272 cm^2 was purchased from Techno Chemics Inc. The facet precision was < 1°. Immediately before its use as the working electrode, the crystal was flame-annealed and quenched by water. A Ag|AgCl electrode in saturated KCl solution served a reference electrode, and a coiled Au wire served a counter electrode in all the electrochemical measurements. The quality of the Au(1 1 1) electrode was examined by comparing its cyclic voltammograms (CV) and differential capacity-potential (*C-E*) curve in 0.05 M $KClO_4$ solution with those in a previous report [43]. The surface roughness, the ratio of real surface area/geometrical area, was found to be less than 1.10 on the basis of the *C-E* curve at negative potentials.

2.2. Electrochemical Measurements

A quartz electrochemical cell was boiled in a sulfuric acid + nitric acid mixture and was rinsed with a copious amount of purified water before use. The reference electrode was set in a separate compartment which was connected to the main compartment through a liquid junction bridge. All the voltammetric and electrochemical fluorescence measurements were made by setting the Au(1 1 1) electrode in a hanging-meniscus (H-M) configuration to the electrolyte solution in an Ar atmosphere (> 99.998%) in a Faraday cage at room temperature (22 ± 2 ℃). We used 0.05 M $KClO_4$ aqueous solution as the base electrolyte solution unless otherwise stated.

HD was deposited on the Au(1 1 1) electrode surface using one of the following two procedures, when necessary with a fluorescence probe.

Procedure 1 (touching method): The Au(1 1 1) single crystal electrode was flame-annealed and quenched by water. This anneal/quench cycle was repeated several times. The electrode while hot after final annealing was cooled to room temperature in the Ar gas flow. The cooled Au(1 1 1) electrode surface was touched to the neat HD liquid/air interface for a period of 10 s, and then dipped in hexane for 10 s. Subsequently, the electrode covered with HD + hexane was placed in a flow of Ar gas (99.998 %) for 10 min to completely evaporate hexane. Incorporation of a probe dye was made by touching of the HD covered electrode surface to 4 μM DPH/hexane solution or 2 μM Pr/hexane solution for a period of 10 s. The electrode was then touched to hexane for 10 s and placed in a flow of Ar gas for 10 min to evaporate hexane.

Procedure 2 (macroscopic casting method): Using a micro-syringe, a defined volume of HD solution in *n*-hexane with dissolved dye at a concentration of 0.02 mol%, when necessary, was placed on a Au(1 1 1) surface immediately after being cooled in Ar gas. It is known that, in the ordered full monolayer of HD molecules on a Au(1 1 1) surface, the area per one HD molecule which is flat-laying in an all-trans conformation with its zig-zag chain plane parallel to the Au surface is 2.2 nm × 0.45 nm [17]. Using this value, we obtained the amount of HD corresponding to 1 ML (ML = monolayer) coverage using the geometrical area of Au(1 1 1) surface to be 0.046 nmol. This amount was applied by casting 10 μL of 4.6 μM HD/hexane solution to prepare 1 ML equivalent coverage, for instance. The deposited amount was increased up to 10000 ML equivalent. The solvent *n*-hexane was allowed to evaporate in a flow of Ar gas for over 10 min before touching to the aqueous electrolyte solution.

As the third procedure, to put one large hanging droplet of neat HD (1 or 3 μL), the droplet was placed using a micro-syringe near the center of the circular Au(1 1 1) electrode surface immediately after being cooled in Ar gas.

The electrode ready for the measurement was set in a H-M configuration by horizontal touching of the electrode to the surface of electrolyte solution in the quartz cell from the Ar gas phase and by subsequent vertical lifting of the electrode so that only the (1 1 1) base surface was in contact with the solution.

Electrode potentials were controlled by a potentiostat (HUSO Electro Chemical System, HECD 9002) connected with a function generator. Differential capacitance-potential (*C*-*E*) curves were obtained from the ac voltammograms assuming an equivalent series circuit of a capacitance of *C* and a resistance. For ac measurements, a lock-in amplifier (EG&G Instruments, model 7256 or 5201) was employed, and the *C*-*E* curves were obtained using an ac modulation at a frequency of 14 Hz with an amplitude of 5 mV_{rms}.

2.3. Electrochemical Fluorescence Microscopic Measurements

An electrochemical fluorescence microscope was set up as shown in Fig. 1. The base of the microscope was a fluorescence microscope eclipse TE300 (Nikon), equipped with 100 W Hg lamp and CCD camera (JAI, 755 Intelligent ICCD Camera) connected by a C-mount. The objective lens was ×10 or ×40 (Nikon, Plan Fluor).

Fig. 1

A Au(1 1 1) electrode with HD on its surface was set in a H–M configuration at a 0.05 M $KClO_4$ solution surface in Ar atmosphere in a newly home-designed quartz cell equipped with a bottom optical window. A glass bottom dish (Matsunami, D111300) was used as the cell bottom window. Fluorescence images were captured by the CCD camera at 30 frame/s.

3. Results and Discussion

Fig. 2

Typical CV and *C*-*E* curve for a Au(1 1 1) electrode in a H-M configuration with HD on its surface deposited by the touching method are shown as solid lines in Fig. 2-a and b. At $E <$ –0.2 V, the *C*-*E* curve ran closely parallel to that at a bare electrode, indicating that the bare Au region was largely exposed to the electrolyte solution. At these potentials, water-insoluble HD occupies only a small fraction of the Au(1 1 1) surface, exhibiting limited decrease of the *C* value from that of a bare electrode Fig. 2-b). The lowest capacitance in the scanned potential range was observed around 0.15 V. The lowest *C* value differed sample-to-sample in the range of 3 μF cm^{-2} to 10 μF cm^{-2}. Assuming that the Au(1 1 1) surface is fully covered by a liquid HD of a homogeneous thickness, *d*, with the static relative dielectric constant of 2.05 [44], these lowest values, if being equated to the interfacial integral capacitances, correspond to d = 0.2 ~ 0.6 nm. Comparison of *d* with the squared radii of gyration of a HD molecule in neat liquid HD, ca. 0.25 nm^2 [45,46] connotes that a thin limit of HD liquid covers the entire Au(1 1 1) surface or the Au surface is imperfectly wetted by liquid HD around pzc of the electrode. Therefore, it should be discarded to estimate the HD coverage only from the capacitance value.

The CV with HD in Fig. 2-a exhibited a couple of current peaks at E_{pn} = –0.08 V on the negative scan and E_{pp} = –0.01 V on the positive scan. These peak potentials were well consistent with the potential range of the steepest change of *C* in the inflection region of the *C*-*E* curve between –0.10 V and 0.05 V. The CV showed a greater capacitive base current level at more negative potentials to the inflection region than the level at more positive potentials, in

harmony with the *C-E* curve. It is most likely that a phase change of HD takes place in this inflection region, because the potential range is near to the order-disorder transition potential reported by He and colleagues for the adsorption monolayer on a Au(1 1 1) electrode surface [17]. Both CV and *C-E* curve were not susceptible to the repeated potential cycling for several hours. This fact also confirms the chemical reversibility of the processes at the interface.

Fig. 2-c and d demonstrate the CVs for the electrodes prepared by the touching method with probe dyes. The addition of DPH did not alter the CV, whereas the addition of Pr resulted in negative shift of order-disorder responses at both E_{pn} and E_{pp}. The details will be discussed later with the fluorescence imaging data.

Fig. 2-e shows the typical CV for a Au(1 1 1) electrode with a 1.0 μL hanging HD droplet after a few potential scan cycles. A couple of capacitive peaks were observed at ca. 0.05 V more positive than those in Fig. 2-a. In the potential region positive of the peak, the capacitive current level was smaller than that at a bare electrode but slightly greater than that in Fig. 2-a. In the potential region negative of the peak, the capacitive current level was almost the same as that at a bare electrode indicating the contacting area of the hanging droplet is inconsiderable. The additional oscillation of the current was most characteristic in this region. It is likely due to stepwise contraction of the contacting area of the 1.0 μL droplet in the negative scan and stepwise increase in the positive scan.

Fig. 3

Surface charge (σ_m)$-E$ curves shown in Fig. 3 were obtained by a potential step train coulometry [47] for a Au(1 1 1) electrode with HD free of probe dye prepared by the touching method. Although the σ_m-E curves were obtained experimentally without any precondition, its analysis was not straightforward, because, as described above, the electrode surface was not necessarily covered by a homogeneous HD adlayer. In such a case, we cannot represent an adlayer by a homogeneous Gibbs excess of the organic molecules in the determinant scale of the surface tension.

The initial potential (E_i) was –0.8 V for the steps to positive direction to obtain the data points for adsorption processes (closed circles in Fig. 3), whereas E_i = 0.4 V for those to negative direction to obtain the points for desorption processes (closed diamonds in Fig. 3). At –0.8 V,

we assume that the coverage of HD is negligibly small to affect the surface charge, based on the *C* values around –0.7 V. Integration of the current transients corrected to the residual current to obtain the change of the surface charge as a function of electrode potential was followed by the pinning of the data to allocate the σ_m value at –0.8 V to be equal to that of a bare electrode. These procedures were described in detail in our previous publication [48].

The $\sigma_m - E$ curves with HD in Fig. 3 displayed a steep slope around –0.15 V. Slight hysteresis because of the step direction was observed, because spreading and desorption processes of HD are accompanied by, respectively, displacement and adsorption of water molecules possessing a large dipole. These features are consistent with the voltammograms in Fig. 2-a and b. The apparent shift of pzc to the positive potential even with a non-polar alkane may originate from slightly preferential orientation of water dipoles to head down hydrogen atoms to the electrode surface in the presence of the HD adlayer.

We first assumed that the $\sigma_m - E$ curve represents homogeneous Gibbs excess on the electrode surface. We tentatively calculated the surface film pressure, $\pi(E)$, by integrating the difference of σ_m between in the presence and absence of HD:

$$\begin{aligned} \pi(E) &= \gamma_{\text{bare}} - \gamma_{\text{HD}} \\ &= \int_{E_f}^{E_i} \sigma_{\text{m}}(E)_{\text{HD}} dE - \int_{E_f}^{E_i} \sigma_{\text{m}}(E)_{\text{bare}} dE \end{aligned} \tag{1}$$

where γ is the surface tension and E_f is the step potential. By setting π(–0.8 V) = 0 mN/m, we found maxima of π as being 48 mN/m at 0.30 V for positive direction measurements for desorption and 40 mN/m at 0.30 V for negative direction measurements for adsorption. Significantly, these values are much lower than the interfacial tension between water and HD at 24.5 ± 0.5ºC, 53.3 mN/m [49]. This result clearly indicated that the electrode is not fully covered by an adsorption film of HD, either by a liquid HD film. On the basis of the Young's equation, prerequisite of the film spreading to completely wet the Au surface is $\pi_{max} > \gamma_{HD/water}$ = 53 mN/m. Because the surface of Au(1 1 1) is rather hydrophilic [50], complete displacement of surface water by HD phase is not allowed.

Fig. 4

Fig. 4 shows typical *in-situ* fluorescence images and fluorescence intensity obtained in the

course of potential cycling at a potential sweep rate (v) of 5 mV s^{-1} for the Au(1 1 1) electrode with HD containing DPH or Pr as fluorescent probe prepared by the touching method. Note that when we deposited the dyes by casting its hexane solution on the Au(1 1 1) electrode without HD followed by evaporation of hexane, the fluorescence image was as dark as of the instrumental background level and potential independent.

First, we describe the results with DPH (Fig. 4-a and b) in reference to corresponding CV in Fig. 2-c. The CV made sure that the addition of DPH did not largely alter the CV in the absence of the dye and that the dye acted actually as "probe" (see also Fig. S2 in Supplementary Data). The fluorescence of the probe dye molecules at a close proximity the metal electrode surface is quenched as a result of reduced lifetime of the excited state. When the probe dye molecules have greater distance from the electrode surface, the fluorescence intensity becomes stronger as a function of the distance [30-38]. If HD stays put on the surface as droplets and its height changes in response to the potential change, the fluorescence intensity depends on the electrode potential. Squeezing of the bottom area of a constant-volume droplet should increase the height of the center of the droplet. Even when a HD + Dye liquid phase of a nanometer-level thickness covers a large area, potential dependent spreading-retracting (in other words, wetting-dewetting) should be observed as the change of the fluorescence image, especially as the change of intensity map. Remind the fact that the shorter the distance between a dye molecule and the metal surface, the greater the fluorescence quenching, as briefly reviewed in the Introduction [30, 35-38]. Therefore, at potentials at which the HD droplet is of bell-shape, it appears as a fluorescent droplet in the image, whereas at the potentials at which the HD is spreading to be a much thinner film, the fluorescent area should be greater but the intensity is substantially quenched. The images in Fig. 4-a clearly show that HD deposited on electrode surface split into a number of droplets as displayed by the light spots. All the light spots in the images were smaller than 50 μm in diameter. The number of light spots increased in negative scan by new appearance of relatively small light spots. The weak light spots present at the positive potentials turned to be brighter spots at negative potentials. In addition, the surroundings of relatively big light spots remained dark even at –0.7 V. We found that almost all the HD droplet in the image exhibited spreading-retracting; the scale of the change for each droplet was smaller than 50 μm (A typical movie is available in a Supplementary Data). A few droplets gathered HD from surroundings, but even this process never produced a droplet greater

than 50 μm in diameter. To sum up, HD does not form a continuous film but splits into many droplets.

The integrated fluorescence intensity, I_{FL}, obtained from the fluorescence image (Fig. 4-a) was plotted as a function of E in Fig. 4-b. To obtain I_{FL}, using the background image in which the difference value was set zero at all the pixels, each pixel in the image of the sample is quantified 256 shades of gray. The summation of the differences of the shade was converted to I_{FL}. To obtain Fig. 4-a and b, we used rather strong excitation light intensity to see the contour clearly. In Fig. 4-b, the steep increase of I_{FL} form ca. 0.0 V in the initial negative scan was in harmony with the increase of the capacitive current (Fig. 2-c and Fig. S-2). I_{FL} took a maximum at –0.19 V, followed by a decline. Although it slightly increased again from –0.4 V to –0.7 V, it decreased monotonically on the positive scan. On the second to the fifth cyclic scans, I_{FL}–E curves ran on the same track as the curve of the positive scan in Fig 4-b, whereas voltammetric curves were superimposable to the first cycle in Fig. 2-c and Fig. S-2. These results revealed a rapid photo-bleaching of the probe dye DPH. Therefore, the images after passing –0.2 V in the first negative scan did not give quantitative brightness of the light spots and values of I_{FL}, while the spatial distributions and outlines of the droplets were quite obvious.

In the use of Pr, obtained CV curve (Fig. 2-d) differed from the curve without dye. On the negative scan, the increase of the capacitive current commenced at –0.1 V and exhibited a peak at E_{pn} = –0.45 V. On the following positive scan, increased capacitive current decayed to –0.1 V after a broad peak around E_{pp} = –0.25 V. In line with the voltammetric behavior, the onset of a steep rise of I_{FL} occurred at –0.3 V on the negative scan (Fig. 4-d, black line). I_{FL} reached a peaked maximum at –0.55 V after the turning of the potential scan, and decayed until 0.20 V was reached. The results of repeated potential scans to record four more cycles (Fig. 4-d) revealed that photo-bleaching was inconsiderable. As far as the fluorescence images (Fig. 4-c) are concerned, although the droplets were smaller than those with DPH, no difference was found in the tendency of potential dependent change of droplet images from the changed observed with DPH. HD did not form a continuous film but split into many droplets smaller than 40 μm in diameter, and the droplets were the brightest around the peak potential, because of the increased height of the top of droplets. The origin of the negative potential shift of the dewetting and squeezing of the droplets with Pr compared with the responses in the absence of a dye and in the presence of DPH is presently undefined. On a speculative bases, the adsorption of Pr molecules

took place at the electrode/droplet interface and resulted in the change of the interfacial tension at the Au(1 1 1)/HD interface. We are currently underway to prove this hypothesis.

In Fig. 4-d, the value of I_{FL} attained its maximum at −0.55 V, whereas capacitive current in CV before and after the maximum was featureless (Fig. 2-d). Important message of this observation is that the fluorescence intensity change is largely due to the droplet height change far beyond the electrochemical double layer thickness region, because the changes in such a far region are hardly reflected in the capacitive current change. Note that the characteristic thickness of the diffuse layer (i.e. the distance to decay the potential drop to be 1/*e* based on the Gouy-Chapman model) in the present experimental condition is ca. 1.3 nm.

To further make sure the absence of continuous spreading HD in a wide surface area even around pzc when using the touching method, we examined the solution redox response of hexacyanoferrate. The use of hexacyanoferrate is well-suited, because its redox potential is near to the pzc.

Four plausible limiting cases should be invoked [51,52] as illustrated in Fig. 5.

Fig. 5

Case 1. HD covers the entire Au surface as a continuous film. The redox reaction of $Fe(CN)^{4-/3-}$ is completely blocked or heavily slowed down to exhibit irreversible CV around $v \sim 10^2$ mV s^{-1}.

Case 2. HD continuous films much wider than the diffusion length, l_D, cover a part of the Au surface, while the other part is HD-free. The waveform of CV is the same as that at a bare electrode, exhibiting the same electrochemical reversibility, but the current scale is factored by less than unity.

Case 3. A continuous film covers the entire surface but has a number of small pores with a uniform diameter smaller than l_D and with the pore-to-pore distance greater than l_D. The waveform of CV of a micro-electrode array is observed. This model was previously used to describe the adsorption film of an insoluble surfactant, 4-pendadecyl pyridine, on a Au(1 1 1) electrode [53].

Case 4. HD stays put on the electrode surface as a number of droplets so that continuous bare Au parts are present on the surface. Unless *v* is so fast to give rise to the contribution of

radial diffusion, the reaction is controlled by planar diffusion. Because the total interconversion rate between two oxidation states is slightly slowed down, a quasi-reversible CV is observed.

In addition, the situation may be potential dependent if the potential region of the redox wave overlaps with the potential dependent change of the state of HD. Note that for the reversible CV of ferricyanide solution, l_D is ca. 5 μm at the cathodic peak potential at v = 100 mV s^{-1} [52].

Fig. 6

Fig. 6 shows CVs obtained in 0.05 mM $K_3[Fe(CN)_6]$ solution for three Au(111) electrodes, a bare Au(1 1 1) and two Au(1 1 1) electrodes with HD; one was prepared by the touching method and the other was with a 3 μL hanging droplet of HD. To avoid the deposition of Fe compound produced in the redox reaction onto the electrode surface, the solution was made be weak alkaline by addition of 2 mM $KHCO_3$. The two electrodes with HD showed quasi-reversible redox reaction of the solution species. In the range of v of 10–100 mV s^{-1}, both anodic and cathodic peak currents (i_{pa} and i_{pc}, respectively) were proportional to $v^{0.5}$. Cases 1 and 3 can be now denied. The slopes of the i_{pa}– $v^{0.5}$ plots were in the order of bare electrode > HD-touching > HD-hanging, where the decrease from the bare electrode to the HD-touching was ca. 10 %.

Fig. 7

Fig. 7 shows a plot of anodic and cathodic peak potentials (E_{pa} and E_{pc}, respectively). The peak separation at v = 10 mV s^{-1} increased from 63 mV at a bare electrode to 77 mV at an electrode prepared by the touching method. The electrode with a hanging droplet showed similar v dependence of the peak potentials to the bare electrode, indicating that the electron transfer rate is not largely retarded compared with that at the bare electrode.

Taken together, the 3 μL hanging HD droplet decreased the bare Au surface exposed to the solution but not the kinetics. The electrode surface area fraction occupied by the droplet was ca. 14 % as a photographical estimation and was close to the extent of the reduction of current. As for the electrode prepared by the touching method, the total area occupied by HD small droplet is much less that 11 % as judged from the decrease of the slope of i_{pa}– $v^{0.5}$ plot. However, the

kinetics as a whole electrode is sluggish. On the basis of combined consideration with the fluorescence image, Case 2 is also denied for the electrode prepared by the touching method. It is unanswered, however, whether an adsorption layer of HD molecules covers the Au surface in the Case 4 around the small droplet peripheries or not.

Fig. 8

We ranged the amount of HD deposited by the casting method up to 10,000 ML equivalent amount. Fig. 8 shows CVs, *C*-*E* curves, and typical fluorescence microscopic images for the HD amounts of 10 ML and 10,000 ML. The fluorescence images taken in the course of negative potential scan were shown. In this measurement, bicarbonate was intentionally added to simultaneously examine its adsorption-desorption. With 10 ML, the lowest *C* value at 0.40 V was 3.0 μF cm^{-2}, indicative of relatively smaller remaining bare Au area. The adsorption process of bicarbonate, giving rise to a sharp adsorption peak at 0.32 V on the positive scan and a desorption peak at 0.28 V on the negative scan at a bare electrode [54], was completely diminished with 10 ML HD. This fact indicates the bare Au part is not adsorbate free, but HD molecules are there to prevent bicarbonate from adsorption. In the fluorescence image, we still find a number of small droplets at 0.4 V, revealing the absence of the formation of a smooth continuous liquid thin adlayer.

With 10,000 ML coverage, the lowest *C* value was 13 μF cm^{-2}, a much greater value than that with 10 ML coverage. Correspondingly, we found larger droplets together with greater total area of dark regions which is most likely the bare gold surface or very thin layer of HD whose top region is still subject to the fluorescence quenching regime. The increase of the number of droplets and brightness of the fluorescence was manifest in the negative potential scan. The size of the droplet was smaller than 30 μm. Together with the *C* value, the Au surface was not covered with a continuous liquid film. With 10,000 ML coverage, bicarbonate adsorption was blocked as in the case of 10 ML coverage.

To sum up, the results in Fig. 8 revealed that even the 10,000 ML equivalent amount of HD does not form a continuous liquid thin adlayer and that the capacitance around pzc became greater with the increase of the amount of HD.

4. Conclusion

We have described potential driven morphological change (reshaping) of insulator alkane liquid droplets on a Au(1 1 1) electrode at a mesoscopic level. Even around the pzc and with even up to 10000 ML equivalent amount of *n*-hexadecane (HD), HD exists as small droplets but never covers the surface as a macroscopic continuous liquid film. When the deposition of HD was made by the touching method, the size of HD droplet observed by fluorescence microscopy was small than 50 μm in diameter. Interestingly, its volume approximately corresponds to the maximal droplet size in ink-jet printing. The large HD/water interfacial tension and highly hydrophilic nature of the Au(1 1 1) surface results in the droplet formation even with a 10000 ML equivalent amount. The total partial area occupied by the droplet is so small that HD on the surface allows quasi-reversible redox reaction of ferricyanide in the solution phase. We also clearly recorded the brightness and size changes of the droplet as seen by fluorescence as well as the integrated fluorescence intensity of the view field. We can conclude that the height of the droplet become greater at more negative potentials. The increment of the height still takes place even after the interfacial capacitance reaches flat region with the capacitance level of a bare electrode. This indicates that the droplet top rising continues at negative potentials beyond the distance gaining the direct control of the double layer structure on the electrode surface. The HD liquid droplets and aqueous electrolyte solution compete with each other to occupy a larger area on the electrode surface. The rise of the droplet top at negative potentials originates in the domination of greater affinity of the Au(1 1 1) surface to water over the affinity to HD. The implication of the disappearance of bicarbonate adsorption, even when the touching method was used, is that a dilute adsorption layer of HD molecules may cover the outer part of the Au surface around the droplets. We are currently under study to precisely quantify the amount of HD deposited by the touching method, to find possible factors to finely regulate the dynamics of the droplet, and to figure out the potential dependent cross section of each droplet.

Acknowledgments

This work was supported by a Grant-in-Aid for Scientific Researches on Innovative Areas

“Molecular Robotics” (No. 24104004 to TS) and a Grant-in-Aid for Challenging Exploratory Research (No. 15K13680 to TS) from The Ministry of Education, Culture, Sports, Science, and Technology, Japan. TS acknowledges very helpful discussion with Prof. Hirohisa Nagatani (presently at Kanazawa University) and Dr. Hironobu Tahara (Nagasaki University) of the *in situ* fluorescence microscopic measurements.

Appendix A. Supplementary Data

Supplementary data associated with this article can be found, in the online version, at http://dx.doi.org/10.1016/j.electacta.2016.XXXXXXX

Content

Fig. S1. Fluorescence and excitation spectra of probe dyes, 1,6-diphenyl-1,3,5-hexatriene (DPH) and perylene (Pr).

Fig. S2. Effect of addition of DPH in *n*-hexadecane on Au(1 1 1) electrode upon the *C-E* curve when touching method was used for deposition.

Video Movie. A typical example of video movie of the fluorescence microscopic image.

References

[1] T. Sagara, Dynamic behaviors of molecular assemblies and nano-substances at electrified interfaces, Chapter 13, in: K. Ariga, H. S. Nalwa (Eds.), Bottom-up Nanofabrication - Supramolecules, Self-Assemblies, and Organized Films, Vol. 3, American Scientific Publishers, Valencia, 2009, pp. 347-373.

[2] M. Chen, I. Burgess, J. Lipkowski, Potential controlled surface aggregation of surfactants at electrode surfaces – A molecular view, Surf. Sci. 603 (2009) 1878-1891.

[3] Th. Wandlowski, Phase transitions in two-dimensional adlayers at electrode surfaces – thermodynamics, kinetics, and structural aspects, in: E. Gileadi, M. Urbakh (Eds.), Encyclopedia of Electrochemistry, Vol. 1, Wiely-VCH, Weinheim, 2003, pp. 383-467.

[4] D. Bizzotto, V. Zamlynny, I. Burgess, C.A. Jeffey, H.-Q. Li, J. Rubinstein, A.R. Merill, J.

Lipkowski, Z. Galus, A. Nelson, B. Pettinger, Amphiphilic and ionic surfactants at electrified interface, Chap. 23, in: A. Wieckowski (Ed), Interfacial Electrochemistry: Theory, Experiment, and Applications, M. Dekker N.Y., 1999, pp. 405-426.

[5] C. Buess-Herman, S. Baré, M. Poelman, M. Van Krieken, Ordered organic adlayers at electrode surfaces, Chap. 24, in: Wieckowski (Ed), Interfacial Electrochemistry: Theory, Experiment, and Applications, A. M. Dekker N.Y., 1999, pp. 427-447.

[6] G. Lippmann, Relations entre les phénomènes électriques et capillaries, Ann. Chim. Phys., 5 (1875) 494-549 (Translation in English: in F. Mugele, J.-C. Baret, Elecctrowetting: from basics to applications, J. Phys.: Condens. Matter 17 (2005) R705-R774.).

[7] N. Inošević, V. Žutić, Spreading and detachment of organic droplets at an electrified interface, Langmuir 14 (1998) 231-234.

[8] B.S. Gallardo, V.K. Gipta, F.D. Eaerton, L.I. Jong, V.S. Craig, R.R. Shah, N.L. Abbott, Electrochemical principles for active control of liquids on submillimeter scales, Science 283 (1999) 57-61.

[9] K. Uosaki, R. Yamada, Formation of two-dimensional crystals of alkanes on the Au(111) surface in neat liquid, J. Am. Chem. Soc. 121 (1999) 4090-4091.

[10] H.M. Zhang, Z.X. Xie, B.W. Mao, X.Xu, Self-assembly of normal alkanes on the Au (111) surfaces, Chem. Eur. J. 10 (2004) 1415-1422.

[11] A. Marchenko, J. Cousty, L. Pham Van, Magic length effects in the packing of n-alkanes adsorbed on Au(111), Langmuir 18 (2002) 1171-1175.

[12] O. Marchenko, J. Cousty, Molecule length-induced reentrant self-organization of alkanes in monolayers adsorbed on Au(111), Phys. Rev. Lett. 84 (2000) 5363-5366.

[13] R. Yamada, K. Uosaki, Two-dimensional crystals of alkanes formed on Au(111) surface in neat liquid. Structural investigation by scanning tunneling microscopy, J. Phys. Chem. B 104 (2000) 6021-6027.

[14] Z.X. Xie, X. Xu, J. Tang, B.W. Mao, Reconstruction-dependent self-assembly of n-alkanes on Au(111) surfaces, J. Phys. Chem. B 104 (2000) 11719-11722.

[15] A. Marchenko, Z. Xie, J. Cousty, L. Pham Van, Structures of self-assembled monolayer of alkanes adsorbed on Au(111) surfaces, Surface Interface Anal. 30 (2000) 167-169.

[16] H.-M. Zhang, J.-W. Yen, Z.-X. Xie, B.-W. Mao, X. Xu, Self-assembly of alkanols on Au(111) surfaces, Chem. Eur. J. 12 (2006) 4006-4013.

[17] Y. He, T. Ye, E. Borguet, The Role of hydrophobic chains in self-assembly at electrified interfaces: observation of potential-Induced transformations of two-dimensional crystals of hexadecane by in-situ scanning tunneling microscopy, J. Phys. Chem. B 106 (2002) 11264-11271.

[18] N. Inošević, V. Žutić, Effect of electrical potential on adhesion, spreading and detachment of organic droplets at an aqueous electrolyte/metal interface, Contact Angle, Wettability and Adhesion, 2 (2002) 1-13.

[19] A.W. Anderson, Physical Chemistry of Surfaces, 5th ed., John Wiley & Sons, New York, Chap 10, 1990.

[20] C.B. Gorman, H.A. Biebuyck, G.M. Whitesides, Control of the shape of liquid lenses on a modified gold surface using an applied electrical potential across a self-assembled monolayer, Langmuir 11 (1995) 2242-2246.

[21] T. Nagai, S. Nakanishi, Y. Nakato, Water molecules adsorbed at electrode surfaces determine the macroscopic contact angles, ChemPhysChem. 8 (2007) 1016-1018.

[22] M. Liu, F. Q. Nie, Z. Wei, Y. Song, L. Jiang, In situ electrochemical switching of wetting state of oil droplet on conducting polymer films, Langmuir 26 (2010) 3993-3997.

[23] R. Yamada, H. Tada, Manipulation of droplets by dynamically controlled wetting gradients, Langmuir 21 (2005) 4254-4256.

[24] A.A. Kornyshev, A.R. Kucernak, M. Marinescu, C.W. Monroe, A.E.S. Sleightholme, M. Urbakh, Ultra-low-voltage electrowetting, J. Phys. Chem. C 114 (2010) 14885-14890.

[25] K. Aoki, P. Tasakorn, Electrode reactions at sub-micron oil|water|electrode interfaces, J. Electroanal. Chem. 542 (2003) 51-60.

[26] S. Casalini, M. Berto, C. A. Bortolotti, G. Foschi, A. Operamolla, M. D. Lauro, O. H. Omar, A. Liscio, L. Pasquali, M. Montecchi, G.M. Farinola, M. Borsari, Electrowetting of nitro-functionalized oligoarylene thiols self-assembled on polycrystalline gold, Appl. Mater. Interfaces 7 (2015) 3902-3909.

[27] J. Zhang, Y. Han, "Dual-parallel-channel" shape-gradient surfaces: toward oriented and reversible movement of water droplets, Langmuir 25 (2009) 14195-14199.

[28] A. Quinn, R. Sedev, J. Ralston, Influence of the electrical double layer in electrowetting, J. Phys. Chem. B 107 (2003) 1163-1169.

[29] W. J. J. Welters, L.G. J. Fokkink, Fast electrically switchable capillary effects, Langmuir 14

(1998) 1535-1538.

[30] D. Bizzotto J. L. Shepherd, Epi-fluorescence microscopy studies of potential controlled changes in adsorbed thin organic films at electrode surfaces, Chap. 3, in: R.C. Alkire, D.K. Kolb, J. Lipkowski, P.N. Ross (Eds.), Advances in Electrochemical Science and Engineering: Diffraction and Spectroscopic Methods in Electrochemistry, Vol. 9, Wiley-VCH Verlag, Weinheim, 2006, pp. 97-126.

[31] D. Bizzotto, J. Lipkowski, Electrochemical and spectroscopic studies of the mechanism of monolayer and multilayer adsorption of an insoluble surfactant at the Au(111)|electrolyte interface, J. Electroanal. Chem. 409 (1996) 33-43.

[32] A. Musgrove, A. Kell, D. Bizzotto, Fluorescence imaging of the oxidative desorption of a BODIPY-alkyl-thiol monolayer coated Au bead, Langmuir 24 (2008) 7881-7888.

[33] J.L. Shepherd, D. Bizzotto, Characterization of mixed alcohol monolayers adsorbed onto a Au(111) electrode using electro-fluorescence microscopy, Langmuir 22 (2006) 4869-4876.

[34] J. Shepherd, Y. Yang, D. Bizzotto, Visualization of potential induced formation of water-insoluble surfactant aggregates by epi-fluorescence microscopy, J. Electroanal. Chem. 524–525 (2002) 54-61.

[35] R.R. Chance, A. Prock, R. Silbey, Molecular fluorescence and energy transfer near interfaces, Adv. Chem. Phys. 37 (1978) 1-65.

[36] Z.-J. Zhang, A.L. Verma, N. Tamai, K. Nakashima, M. Yoneyama, K. Iriyama, Y. Ozaki, Excitation energy transfer in Langmuir–Blodgett films of 5-(4-N-octadecylpyridyl)-10,15,20-tri-p-tolylporphyrin on gold-evaporated glass substrates studied by time-resolved fluorescence spectroscopy, Thin Solid Films 333 (1998) 1-4.

[37] K. Tawa, K. Morigaki, Substrate-supported phospholipid membranes studied by surface plasmon resonance and surface plasmon fluorescence spectroscopy, Biophys J. 89 (2005) 2750–2758.

[38] R. Rossetti, L.E. Brus, Time resolved energy transfer from electronically excited $^3B_{3u}$ pyrazine molecules to planar Ag and Au surfaces, J. Chem. Phys. 76, 1146-1149 (1982).

[39] P.T. Leung, T.F. George, Energy-transfer theory for the classical decay rates of molecules at rough metallic surfaces, Phys. Rev. B 36 (1987) 4664-4671.

[40] C. Amatore, S. Arbault, Y. Chen, C. Crozatier, F. Lemaitre, Y. Verchier, Coupling of electrochemistry and fluorescence microscopy at indium tin oxide microelectrodes for the

analysis of single exocytotic events, Angew. Chem. Int. Ed. 45 (2006) 4000-4003.

[41] F. Pak, K. Meral, R. Altundas, D. Ekinci, Self-assembled monolayers of fluorene- and nitrofluorene-terminated thiols on polycrystalline gold electrode: Electrochemical and optical properties, J. Electroanal. Chem. 654 (2011) 20-28.

[42] Z.L. Yu, J. Casanova-Moreno, I. Guryanov, F. Maran, D. Bizzotto, Influence of surface structure on single or mixed component self-assembled monolayers via in situ spectroelectrochemical fluorescence imaging of the complete stereographic triangle on a single crystal Au bead electrode, J. Am. Chem. Soc. 137 (2015) 276-288.

[43] A. Hamelin, Cyclic voltammetry at gold single-crystal surfaces. Part 1. Behaviour at low-index faces, J. Electroanal. Chem. 407 (1996) 1-11.

[44] W.M. Haynes CRC Handbook of Chemistry and Physics, 91th Edition, Taylor & Francis, 2010.

[45] H.-C. Tseng, R.-Y. Chang, J.-S. Wu, Molecular structure property and potential energy dependence on nonequilibium-thermodynamic state point of liquid n-hexadecane under shear, J. Chem. Phys. 134 (2011) 044511-1-12.

[46] C.T. Cui, S.A. Gupta, P.T. Cummings, H.D. Cochran, Molecular dynamics simulations of the rheology of normal decane, hexadecane, and tetracosane, J. Chem. Phys. 105 (1996) 1214.

[47] J. Lipkowski, L. Stolberg, Molecular adsorption at gold and silver electrodes, Chap. 4, in: J. Lipkowski, P.N. Ross (Eds.), Adsorption of Molecules at Metal Electrodes, VCH, N.Y., 1992, pp. 171-238.

[48] K. Uematsu, T. Sagara, Voltammetric study of adsorption layers of various 4-pyridyl terminated surfactants on a Au(111) electrode: Effects of electronic property of pyridyl group and intermolecular hydrogen bonding upon potential-driven phase changes, J. Electroanal. Chem. 623 (2008) 109-119.

[49] R.E. Johnson, Jr., R.H. Dettre, The wettability of low-energy liquid surfaces, J. Colloid Interface Sci. 21 (1966) 610-622.

[50] J. Lipkowski, C. Nguyen Van Huong, C. Hinnen, R. Parsons, J. Chevalet, Adsorption of diethylether on single-crystal gold electrodes: Calculation of adsorption parameters, J. Electroanal. Chem. 143 (1983) 375-396.

[51] C. Amatore, Electrochemistry at ultramicroelectrodes, Chap. 4, in: I. Rubinstein (Ed.),

Physical Electrochemistry: Principles, Methods and Applications, Marcel Dekker N.Y., 131-208 (1995).

[52] R.C. Compton, C.E. Banks, Understanding Voltammetry, World Scientific, Singapore (2007).

[53] D. Bizzotto, A. McAlees, J. Lipkowski, R. McCrindle, Barrier properties of a thin film of 4-pentadecylpyridine coated at Au(111) electrode surface, Langmuir 11 (1995) 3243-3250.

[54] K. Arihara, F. Kitamura, T. Ohsaka, K. Tokuda, Characterization of the adsorption state of carbonate ions at the Au(111) electrode surface using in situ IRAS, J. Electroanal. Chem. 510 (2001) 128-135.

Figure captions

Fig. 1. Schematic depiction of the electrochemical fluorescence microscope setup and spectroelectrochemical cell used in the present study.

Fig. 2. Collection of voltammetric data for various Au(1 1 1) electrodes in contact with 0.05 M $KClO_4$ aqueous solution (v are given in each panel): Panels (a) and (b) show typical CV (a) and *C-E* curve (b) for a Au(1 1 1) electrode with HD on its surface deposited by the touching method (The gray lines are the data for a bare Au(1 1 1) electrode.) Panels (c) and (d) exhibit thick-line CVs with HD containing DPH (c) and Pr (d), and gray-line CV with HD containing no dye. Panel (e) shows CV for a Au(1 1 1) electrode with 1.0 μL hanging HD droplet (thick line) in comparison with CV for a Au(1 1 1) electrode with HD on its surface deposited by the touching method (gray line).

Fig. 3. $\sigma_m - E$ curves obtained by a potential step train coulometry for a Au(1 1 1) electrode with HD on its surface deposited by the touching method in contact with 0.05 M $KClO_4$ solution. The initial potential, E_i, which is the basal potential for the step train, was –0.8 V for the steps to positive direction to record the adsorption process, whereas E_i = 0.4 V for the steps to negative direction to record the desorption process. The $\sigma_m - E$ for a bare Au(1 1 1) electrode in the absence of HD is also shown by triangles.

Fig. 4. Fluorescence images obtained in the course of in-situ potential cycling at v = 5 mV s^{-1} with (a) DPH and (c) Pr, and integrated intensity (I_{FL})-potential (E) curves with (b) DPH and (d) Pr obtained by integrating one screen of the entire fluorescence microscopic images obtained at v = 5 mV s^{-1}. The excitation wavelength range was 355 – 375 nm for both DPH and Pr. The detecting wavelength range was 395 – 700 nm for both DPH and Pr. The diameter of circular viewing field in (a) and (b) is 1020 mm. In (d), $I_{FL} - E$ curves for continuous five repeated cyclic scans are shown where the order of the lines is black-red-blue-green-gray in color (in gray scale, the first scan is the thickest line and the 5th scan is the thinnest one).

Fig. 5. Schematic models for the solution redox response of hexacyanoferrate. For details,

see text.

Fig. 6. CVs at v = 10 mV s^{-1} for a Au(1 1 1) electrodes with HD prepared by the touching method (upper panel) and by depositing one 3 μL droplet (lower panel) for the solid lines in 0.50 mM $K_3[Fe(CN)_6]$ + 2 mM $KHCO_3$ + 50 mM $KClO_4$ aqueous solution. Gray lines were CV for a bare Au(1 1 1) electrode.

Fig. 7. Plots of peak potentials (E_{pa} and E_{pc}, see text) for CV obtained in 0.50 mM $K_3[Fe(CN)_6]$ + 2 mM $KHCO_3$ + 50 mM $KClO_4$ aqueous solution at a bare Au(1 1 1) electrode (close square), with HD prepared by touching method (closed circle), and with one 3 μL droplet of HD (open circle).

Fig. 8. CV (upper) and *C-E* curve (lower) for a Au(1 1 1) electrode with HD (10 ML, and 10,000 ML with dissolved Pr as the fluorescence probe dye) on its surface deposited by the macroscopic casting method, in 50 mM $KClO_4$ + 2 mM $KHCO_3$ solution. Sweep rate (v) for CV was 20 mV s^{-1}. *In situ* fluorescence images HD micro-droplet on Au(1 1 1) electrode surface are shown at the right hand side.

Fig.1

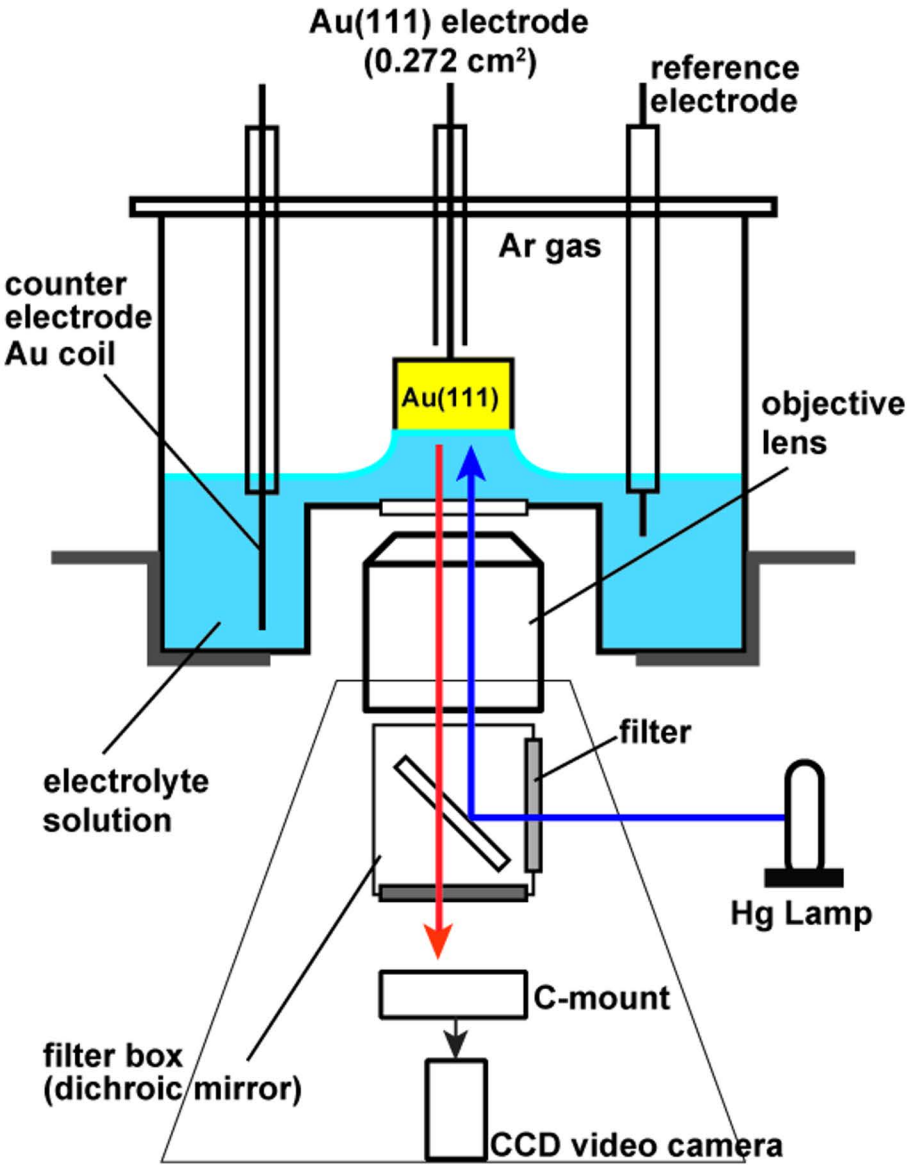
Au(111) electrode
(0.272 cm²)
reference
electrode
Ar gas
counter
electrode
Au coil
Au(111)
objective
lens
electrolyte
solution
filter
Hg Lamp
C-mount
filter box
(dichroic mirror)
CCD video camera

Fig.2

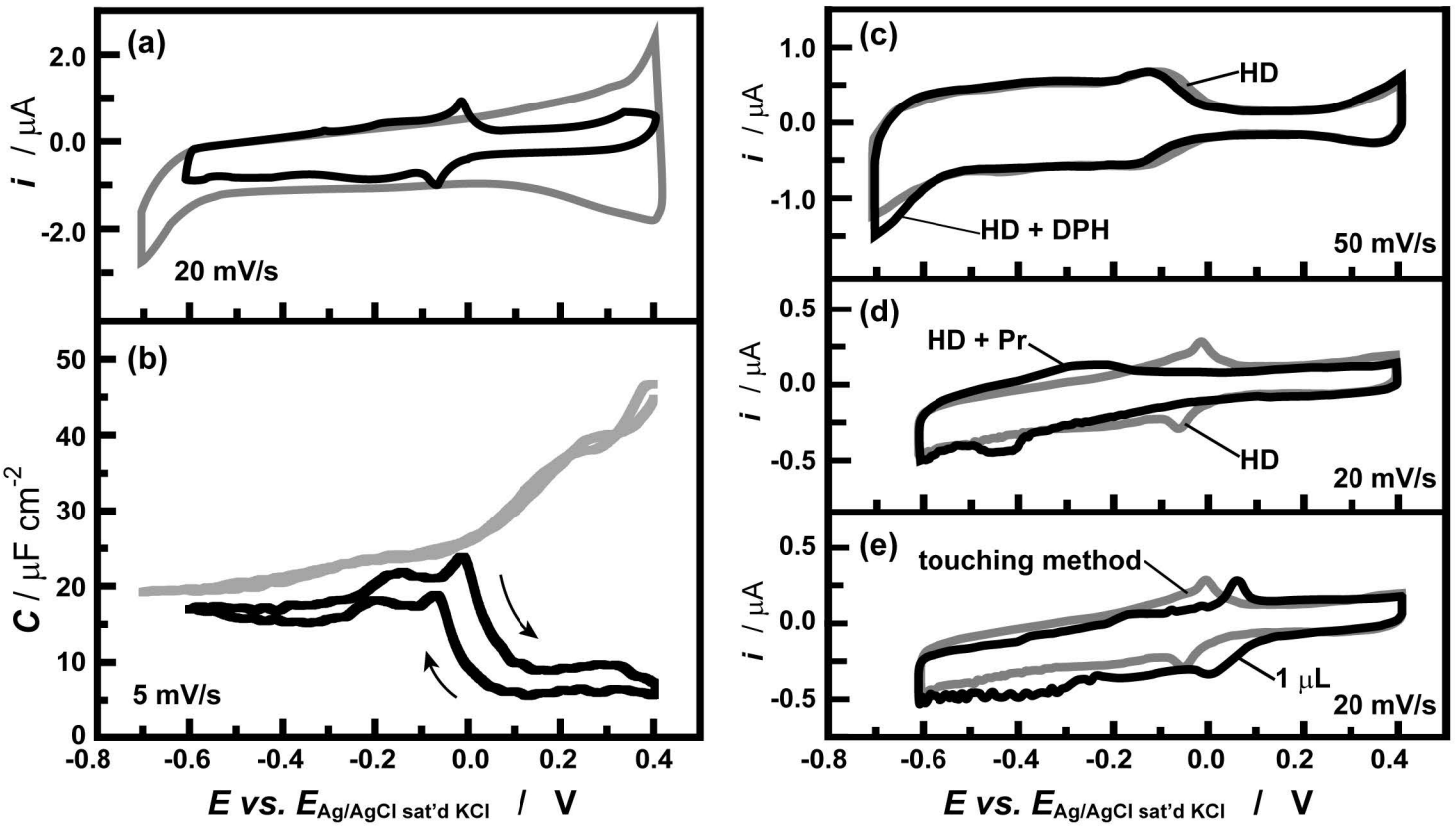
(a)
20 mV/s
(b)
5 mV/s
(c)
HD
HD + DPH
50 mV/s
(d)
HD + Pr
HD
20 mV/s
(e)
touching method
1 μL
20 mV/s
i / μA
C / μF cm-2
E vs. EAg/AgCl sat'd KCl / V

Fig.3

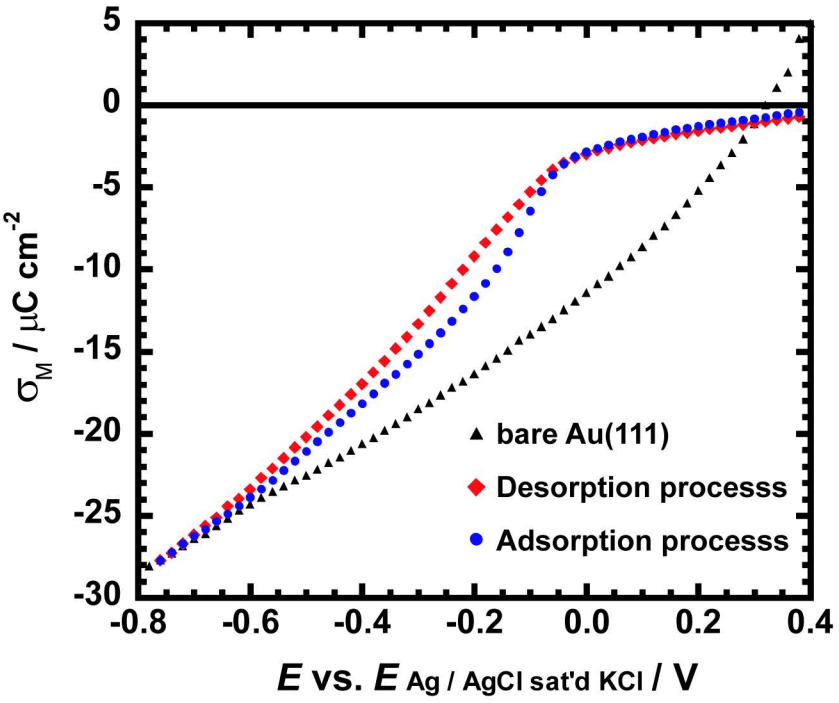
5
0
-5
-10
-15
-20
-25
-30
-0.8
-0.6
-0.4
-0.2
0.0
0.2
0.4
σM / μC cm-2
E vs. E Ag / AgCl sat'd KCl / V
bare Au(111)
Desorption processs
Adsorption processs

Fig.4

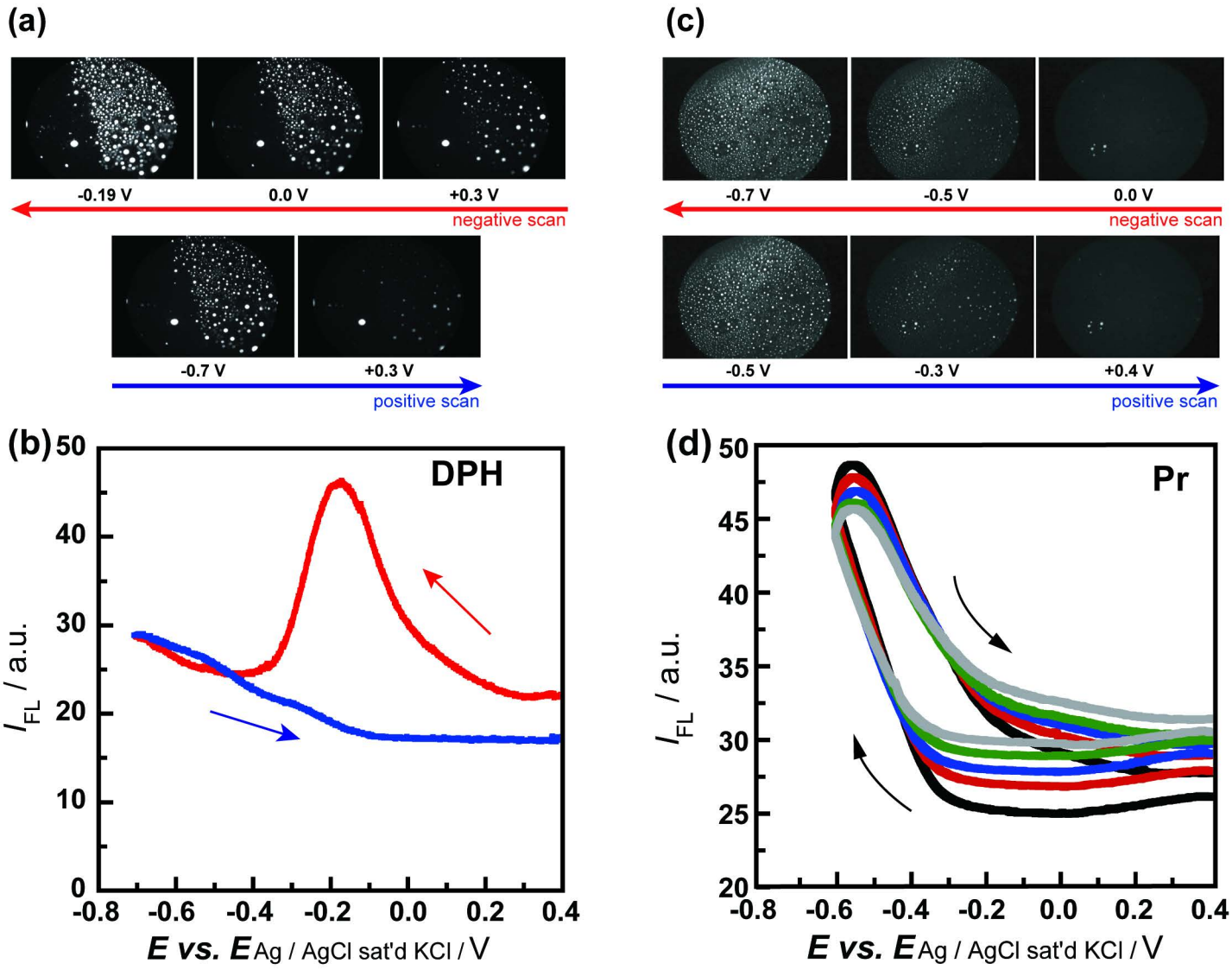
(a)
-0.19 V
0.0 V
+0.3 V
negative scan
-0.7 V
+0.3 V
positive scan
(c)
-0.7 V
-0.5 V
0.0 V
negative scan
-0.5 V
-0.3 V
+0.4 V
positive scan
(b)
DPH
I_{FL} / a.u.
E vs. E Ag / AgCl sat'd KCl / V
(d)
Pr
I_{FL} / a.u.
E vs. E Ag / AgCl sat'd KCl / V

Fig.5

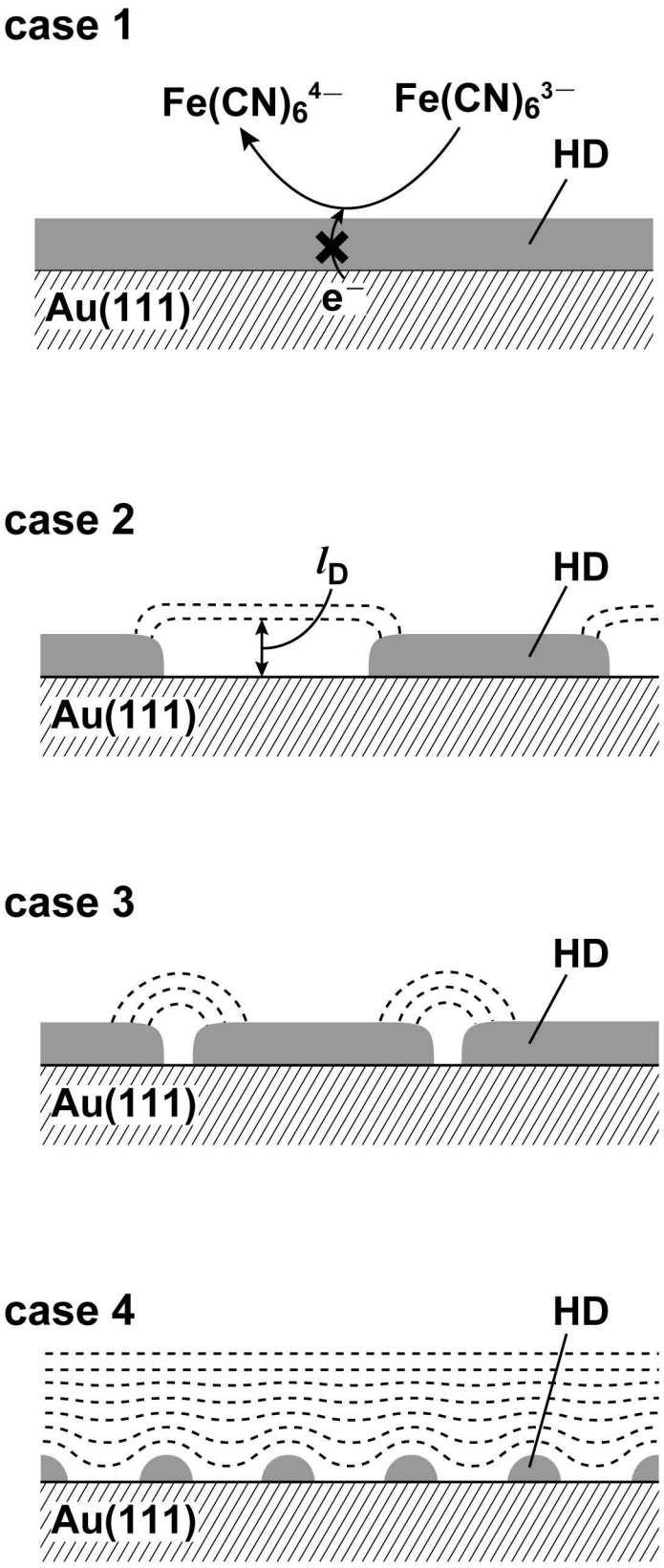
case 1
$Fe(CN)_6^{4-}$
$Fe(CN)_6^{3-}$
HD
e^-
Au(111)
case 2
l_D
HD
Au(111)
case 3
HD
Au(111)
case 4
HD
Au(111)

Fig.6

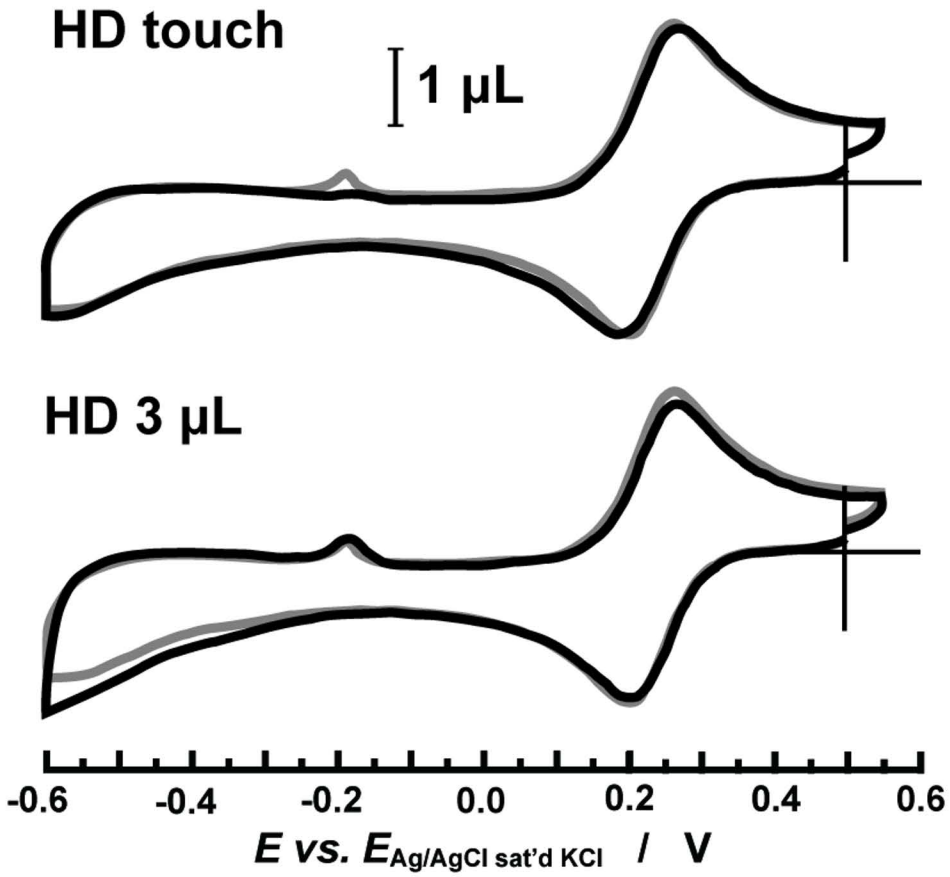

Fig.7

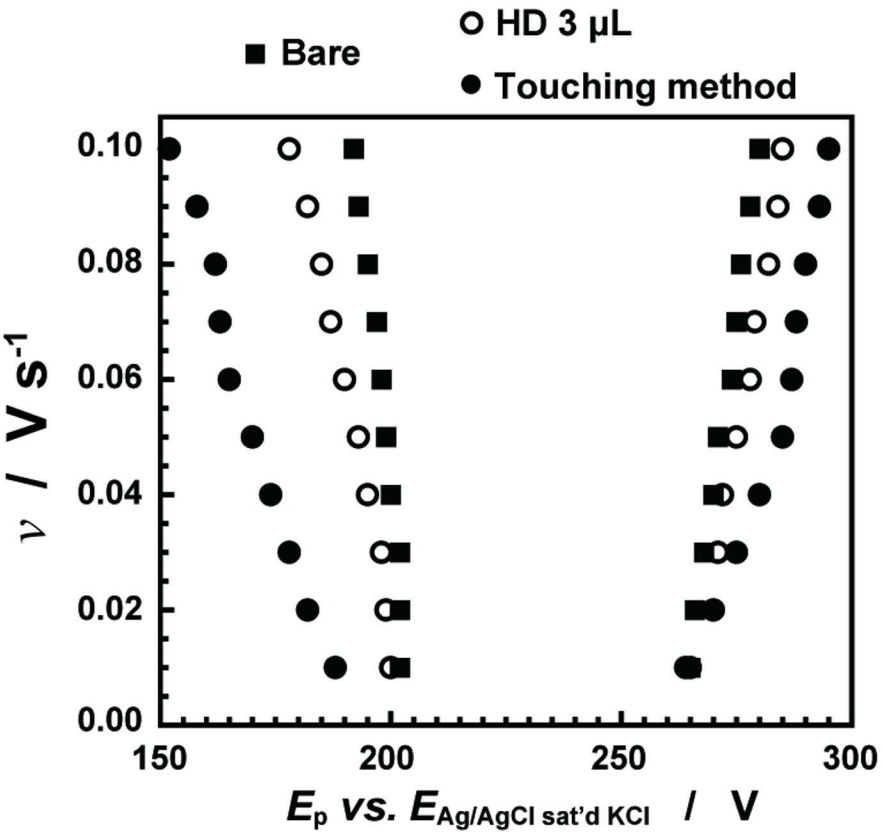
Bare
HD 3 μL
Touching method
0.10
0.08
0.06
0.04
0.02
0.00
ν / V s-1
150
200
250
300
Ep vs. EAg/AgCl sat'd KCl / V

Fig.8

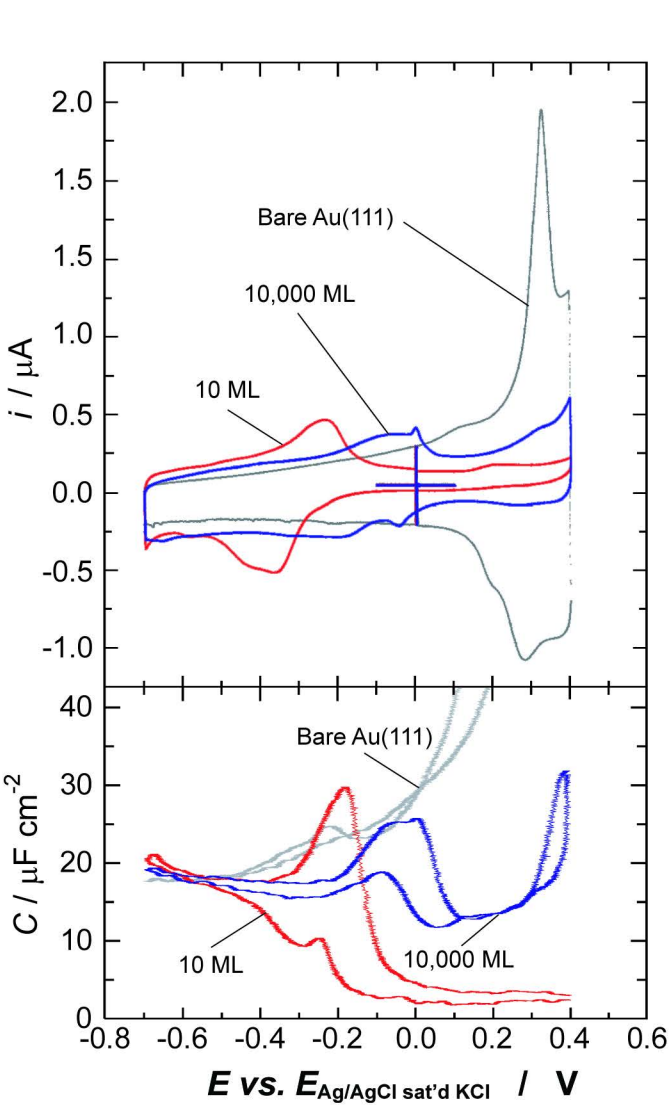
Bare Au(111)
10,000 ML
10 ML
i / μA
C / μF cm-2
E vs. EAg/AgCl sat'd KCl / V

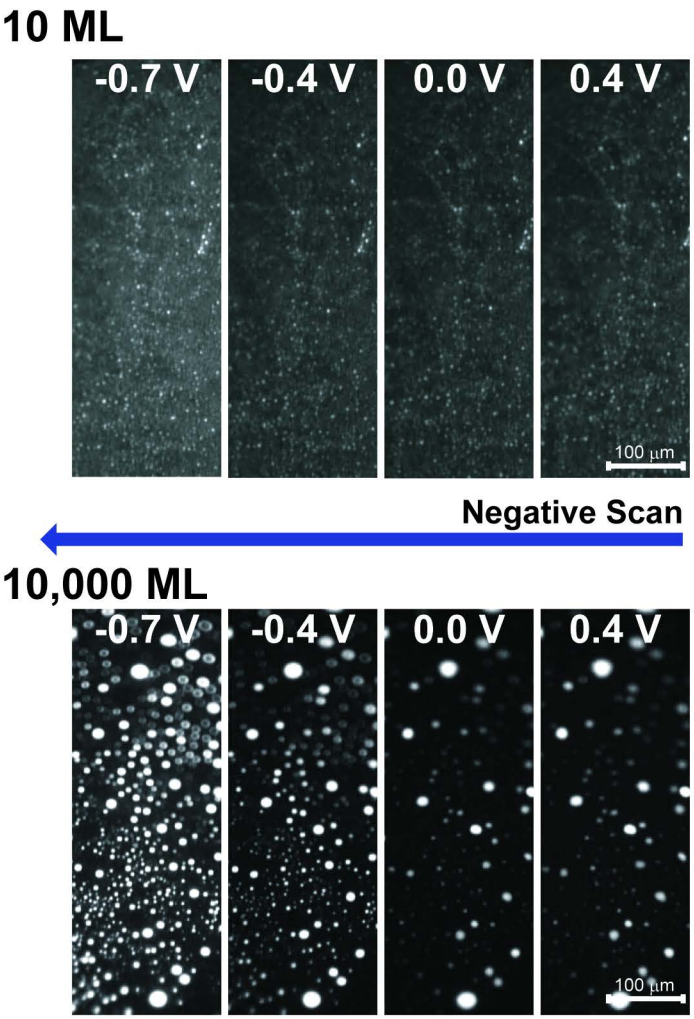
10 ML
-0.7 V
-0.4 V
0.0 V
0.4 V
100 μm
Negative Scan
10,000 ML
-0.7 V
-0.4 V
0.0 V
0.4 V
100 μm

Graphical abstract